Fine-structure analysis of spin-polarized low-energy electron diffraction from W(001)

R. O. Jones
Institut für Festkörperforschung der Kernforschungsanlage Jülich, D-5170 Jülich, Federal Republic of Germany

P. J. Jennings
School of Mathematical and Physical Sciences, Murdoch University, Murdoch WA 6150, Australia

(Received 26 July 1982)

The theory of spin-polarized low-energy electron diffraction (LEED) is used to analyze the observed fine structure in experimental data for W(001). Within a spin-dependent scattering model, a saturated image barrier provides a satisfactory description, and the analysis leads to a model of the surface potential barrier for W(001). Simpler models, such as those commonly used for LEED intensity calculations, are unable to reproduce all of the observed structure. The complex fine structure of the spin-polarized LEED intensity curves is interpreted in terms of the interaction between Bragg peaks, spin-dependent features, and barrier scattering effects. Resonance effects do not need to be invoked.

I. INTRODUCTION

Although low-energy electron diffraction (LEED) is one of the most widely used methods for obtaining structural information about surfaces, the use of spin-polarization effects is a relatively recent innovation. The development of sources capable of producing highly polarized electron beams[1,2] has now permitted the application of the technique, the basic theory for which was developed more than a decade ago.[3,4] Feder[5] has shown that the additional information contained in LEED spin-polarization profiles is a valuable aid in structural analysis of heavy-metal surfaces. Pierce *et al.*[6] have recently published spin-polarized data for W(001) at low energies and in this paper we interpret the structure of their curves and show their value in surface-barrier analysis.[7,8]

The structure of LEED intensity curves from W(001) for electrons of low energy and low angles of incidence has been the subject of much discussion in recent years. Particularly striking are a narrow feature at about 4 eV, which persists over a range of incident angles,[9] and a remarkable asymmetry between spin-up and spin-down intensities for angles of incidence θ near 15°.[6] The latter feature, a double peak in the spin-up intensity with a single peak in the spin-down channel, has been attributed by Malmström and Rundgren[10] to a particular form of threshold effect, namely interacting surface resonances. McRae *et al.*[6] analyzed these data in terms of resonances and interference effects.

Threshold effects and, in particular, surface-barrier resonances are well-studied features of LEED fine structure.[11] Their origin is in the backscattering of nonspecular beams by the surface barrier and their recombination with the beam specularly reflected from the substrate[12] (see Fig. 1). Nonspecular beams require a certain threshold energy to emerge into the vacuum and the most striking effects, usually in the form of a series of narrow peaks in the specular intensity curve, occur just below this energy.[13] The scattering at the surface barrier plays an important role in the formation of the fine structure and Echenique and Pendry[14] provided criteria on this scattering for the occurrence of surface-barrier resonances. Le Bosse *et al.*[15] have shown, however, that these criteria are seldom satisfied and confirm the assessment of Dietz *et al.*[16] that thresh-

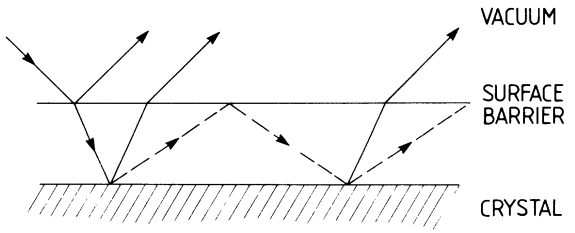

FIG. 1. Mechanism of threshold structure due to barrier scattering in LEED. Full lines indicate the specular beam and the broken lines a preemergent beam which is totally internally reflected by the surface barrier. The figure shows the interaction between the (00) and (10) beams. In the experiment discussed here, the effects arise from the (00) and ($\bar{1}$0) beams.

old features are more accurately described as interferences or coupling between two diffracted beams. We therefore use the term (spin-polarized) LEED fine structure to describe them. Some years ago, we performed model calculations[17] which showed that this fine structure should also be present in spin-polarized LEED, but that spin-up and spin-down peaks may be displaced slightly by spin-orbit effects in the atomic potential. This prediction was confirmed by the work of Pierce *et al.*[6]

LEED fine structure has been measured in Cu, Ni, and W.[18,19] Its sensitivity to the form of the surface barrier means that its analysis can provide information about the scattering potential for electrons near surfaces,[18] an essential input for calculations of electron states at surfaces. There have been numerous discussions of the barrier for idealized models of metal surfaces,[20,21] and Lang and Kohn[21] showed that the potential far from a jellium surface has the form

$$V(z)=-1/[2(z-z_0)]\ , \tag{1}$$

in rydberg units, where z_0 denotes the center of mass of the image charge. In analyzing the Cu(001) fine structure, Dietz *et al.*[16] assumed the asymptotic form (1), with z_0 being an adjustable parameter. Nearer the surface, the image potential "saturates" rather than becoming infinitely attractive at $z=z_0$, and Dietz *et al.*[16] used a linear continuation to the jellium edge, where the potential has the value $-U_1$ (see Fig. 2). They found that a line of values in the parameter space (z_0,U_1) was consistent with the experimental data for Cu(001).

In this paper, we analyze the W(001) fine structure present in the spin-polarized LEED data of Pierce *et al.*[6] and the high-resolution LEED measurements of Adnot and Carette.[19] The barrier we assume is also described by the parameters (z_0,U_1), but is continued linearly to the point where it joins continuously the crystal inner potential $(-U_0)$. This construction avoids the discontinuities in the fine-structure profiles produced if the barrier is truncated at the outermost layer $z=0$. The saturated image barrier is one-dimensional and necessarily approximate. However, it allows for two essential features, the translation of the image plane and barrier saturation.

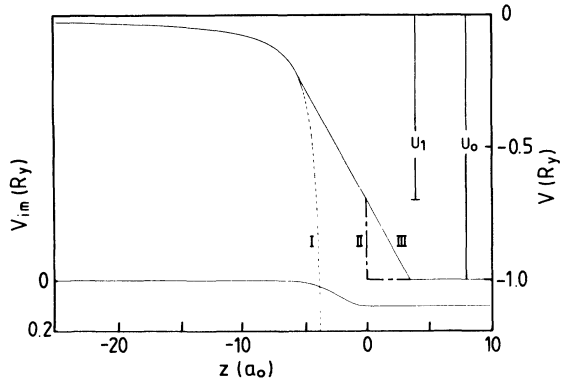

FIG. 2. Surface barriers with image plane (z_0) located at $z=-3.3$ bohr. I: classical image barrier. II: form used in Ref. 16, with discontinuity at $z=0$. III: form used in present calculation. V_{im} denotes the imaginary part of the barrier potential.

In Sec. II we review the experiments which are the basis of the present analysis and in Sec. III describe the details of our method of calculation. In Sec. IV we indicate how we determine the barrier parameters and, in Sec. V, discuss the origin of the fine structure at low angles of incidence. The results we obtain are summarized in Sec. VI.

II. EXPERIMENTAL DATA TO BE ANALYZED

A. Spin-polarized LEED

The data of Pierce *et al.*[6] were collected in a LEED apparatus containing a GaAs source which produced spin-polarized electrons by photoemission with circularly polarized light. The spin-polarization obtained is 43% and its direction is changed by reversing the direction of rotation of the light polarization. In the experiment,[1] Pierce *et al.* modulated the spin-direction in the incident beam and used a lock-in amplifier to measure the specularly reflected alternating current synchronous with the modulation. They also measured the direct-current component of the scattered intensity and calculated the Sherman function S as the ratio of the ac to the dc signal divided by the magnitude of the polarization of the incident beam $|P_0|$,

$$S=\frac{1}{|P_0|}\frac{I_\uparrow-I_\downarrow}{I_\uparrow+I_\downarrow}\ . \tag{2}$$

$I_\uparrow$ and $I_\downarrow$ are the scattered intensities for incident beams with up and down spin-polarizations with respect to the scattering plane.

The intensity of scattering for hypothetical 100% spin-polarized incident beams can be found from the Sherman function using

$$I_\uparrow=I_0(1+S)\ , \tag{3}$$

$$I_\downarrow=I_0(1-S)\ , \tag{4}$$

where

$$I_0=(I_\uparrow+I_\downarrow)/2\ . \tag{5}$$

The data were collected for W(001) at a temperature between 500 and 600 °C to ensure that the surface

had a (1×1) periodicity. The intensity curves were collected over the range 0—12 eV with an energy resolution of 130 meV and for angles of incidence θ between 15° and 43° along the (01) azimuth.

B. LEED measurements

High-resolution LEED data from W(001) have been reported by Adnot and Carette[19] for $\theta=48°$ along the (01) azimuth, with energies between 0 and 7 eV. The energy resolution was 15 meV and the angular resolution better than 0.8°. The threshold fine structure is clearly resolved and the peak splittings are known accurately.

LEED intensity curves for incident energies below 20 eV have been obtained at normal incidence by Khan *et al.*[22] and by Herlt *et al.*[23] The latter data have been obtained using crossed $\vec{E}$ and $\vec{B}$ fields and have a resolution of approximately 20 meV. The angular resolution is less satisfactory, however, and there is no evidence of any fine structure in the published data. The two sets of data[22,23] are rather similar and will prove useful in interpreting the low-energy and low-angle structure in the LEED intensity profiles.

III. METHOD OF CALCULATION

A. Spin-polarized LEED

Consider a single electron beam incident on a surface barrier giving rise to N diffracted beams. The reflection coefficient matrix $\underline{R}_T^{-+}$ for the crystal may be expressed as[13]

$$\underline{R}_T^{-+}=\underline{r}^{-+}+\underline{t}^{--}\underline{R}^{-+}(\underline{1}-\underline{r}^{+-}\underline{R}^{-+})^{-1}\underline{t}^{++}\,, \tag{6}$$

where (see Fig. 3) $\underline{r}^{-+}$ is the reflection matrix for the incoming beams at the barrier, $\underline{t}^{--}$ is the transmission matrix for the outgoing beam at the barrier, $\underline{R}^{-+}$ is the reflection matrix for the substrate, $\underline{r}^{+-}$ is the internal reflection matrix for the surface barrier, and $\underline{t}^{++}$ is the transmission matrix for the incoming beams at the barrier. The crystal fills the halfspace $z>0$ and we use the convention that $\underline{r}^{-+}$, for example, describes the scattering of an electron moving in the direction of $z>0$ into the direction of $z<0$. In general, $\underline{r}^{-+}$ is small except at very low energies and may be neglected. Owing to inelastic scattering, the diagonal elements of $\underline{R}^{-+}$ are much smaller than unity and the matrix inverse in Eq. (6) can be expanded as follows:

$$(\underline{1}-\underline{r}^{+-}\underline{R}^{-+})^{-1}=\underline{1}+\underline{r}^{+-}\underline{R}^{-+}+\cdots\,, \tag{7}$$

so that

$$\underline{R}_T^{-+}\simeq\underline{t}^{--}\underline{R}^{-+}\underline{t}^{++} +\underline{t}^{--}\underline{R}^{-+}\underline{r}^{+-}\underline{R}^{-+}\underline{t}^{++}\,. \tag{8}$$

As illustrated in Fig. 3, this expression includes all scattering effects up to second order, and Dietz *et al.*[16] found this to be an adequate approximation for Cu(001). We have tested it for W(001) and find that the higher-order terms are indeed negligible due to inelastic scattering. We also find that the evanescent beams can be neglected in the barrier region because they decay rapidly and contribute very little to the calculated intensities.

LEED fine structure therefore arises from second-order scattering involving total internal reflection of a diffracted beam at the surface barrier, subsequent diffraction back into the specular beam, and transmission through the barrier. These features, more properly described as interferences rather than resonances, produce a series of peaks (sometimes called "Rydberg series") converging on the emergence of a new diffracted beam into the vacuum. Other features in the intensity curves which arise from constructive interference in scattering from the bulk crystal are known as Bragg peaks. Barrier scattering can redistribute intensity between beams, and Bragg peaks in preemergent beams can produce corresponding maxima in the LEED fine structure. Such features are usually broader than the peaks in the Rydberg series and are most evident when they are somewhat removed from the emergence energy.

For spin-polarized LEED with N diffracted beams, the scattering matrices in Eq. (8) will have the dimensions $2N\times2N$, as each beam has both spin-up and spin-down components. The scattered beams are then composed of spin ensembles of the form

$$\psi_i=e^{i\vec{k}\cdot\vec{r}}\begin{bmatrix}U_1^i\\U_2^i\end{bmatrix}\,, \tag{9}$$

where U_1^i and U_2^i are the spin-up and spin-down projections of the ith spin ensemble of the beam. The matrix $\underline{R}_T^{-+}$ contains a set of 2×2 submatrices $\underline{M}$ which link the incoming specular beam ψ_0 to the

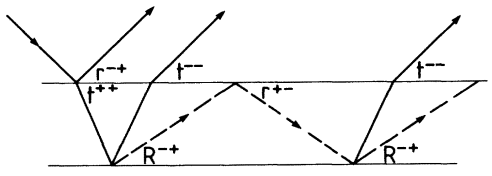

FIG. 3. Contributions to total scattering matrix [see Eq. (6) and Fig. 1].

outgoing beam ψ' as follows:

$$\psi_i' = \underline{M}\psi_{0i} \ . \tag{10}$$

The density matrix $\underline{\rho}'$ for a scattered beam is given by a sum over the N spin ensembles,

$$\begin{aligned}\underline{\rho}' &= \frac{1}{N}\sum_{q=1}^{N}\psi_q'\psi_q'^{\dagger} \\ &= \underline{M}\underline{\rho}_0\underline{M}^{\dagger} \\ &= \tfrac{1}{2}\underline{M}(\underline{1}+\underline{P}\cdot\underline{\sigma})\underline{M}^{\dagger} \ ,\end{aligned} \tag{11}$$

where $\underline{\rho}_0$ is the density matrix of the primary beam. The intensity of the diffracted beam is given by

$$I = \mathrm{Tr}(\underline{\rho}') \tag{12}$$

and the polarization by

$$\underline{P}' = \mathrm{Tr}(\underline{\rho}'\underline{\sigma})/\mathrm{Tr}(\underline{\rho}') \ , \tag{13}$$

where $\underline{\sigma} = \underline{i}\sigma_x + \underline{j}\sigma_y + \underline{k}\sigma_z$ and $\sigma_x, \sigma_y, \sigma_z$ are the Pauli spin matrices. The density matrix of the primary beam is given by

$$\begin{aligned}\underline{\rho}_0 &= \tfrac{1}{2}(\underline{1}+\underline{P}_0\cdot\underline{\sigma}) \\ &= \frac{1}{2}\begin{pmatrix} 1+P_{0z} & P_{0x}-iP_{0y} \\ P_{0x}+iP_{0y} & 1-P_{0z} \end{pmatrix}\end{aligned} \tag{14}$$

in general, and

$$\underline{\rho}_0 = \tfrac{1}{2}\underline{1}$$

for an unpolarized primary beam. In the present calculations we have assumed that the incident beam is totally polarized in either the spin-up or spin-down state. Since the z axis is perpendicular to the crystal and the primary beam is incident along the x axis, the scattering plane is the xz plane. Therefore,

$$\underline{\rho}_0^{\uparrow} = \frac{1}{2}\begin{pmatrix} 1 & -i \\ i & 1 \end{pmatrix}$$

and (15)

$$\underline{\rho}_0^{\downarrow} = \frac{1}{2}\begin{pmatrix} 1 & i \\ -i & 1 \end{pmatrix} .$$

The scattered intensities for the specular beam can then be found from Eqs. (11) and (12).

B. Scattering by the substrate

The substrate scattering matrix $\underline{R}^{-+}$ is calculated with the use of the layer Korringa-Kohn-Rostoker (KKR) procedure of Kambe[24] and the transfer matrix method of McRae.[25] This is a similar approach to that taken in most other theories of LEED. The spin-dependent layer KKR procedure has been described in detail elsewhere.[3] The amplitude reflection and transmission coefficients for a single layer are obtained by solving a set of linear equations whose coefficients depend on the atomic scattering of the substrate. These phase shifts are obtained by solving the Dirac equation for the W muffin-tin potential of Mattheiss[26] using the program of Bunyan and Schonfelder.[27] This program is widely used in spin-polarized LEED calculations for this purpose. The scattering between the muffin-tin spheres is treated as described previously.[28]

The reflection and transmission coefficients so obtained are used to construct a reduced transfer matrix $\underline{R}$ for the semi-infinite solid. This matrix is then diagonalized by a matrix transformation $\underline{T}^{-1}\underline{R}\,\underline{T}$ and the backscattered amplitudes $\underline{b}_0$ from the substrate calculated from the primary amplitudes $\underline{a}_0$ using

$$\begin{aligned}\underline{b}_0 &= -\tilde{\underline{T}}_{22}^{-1}\tilde{\underline{T}}_{21}\underline{a}_0 \\ &= \underline{R}^{-+}\underline{a}_0 \ .\end{aligned} \tag{16}$$

$\tilde{\underline{T}}_{22}$ and $\tilde{\underline{T}}_{21}$ are the $2N\times 2N$ submatrices of $\underline{T}^{-1}$, where N is the number of diffracted beams. The substrate scattering matrix $\underline{R}^{-+}$ is then used in Eq. (8) to calculate the spin-polarized LEED profiles.

C. Scattering by the surface barrier

The barrier reflection and transmission matrices $\underline{r}$ and $\underline{t}$ required in Eq. (8) are obtained by solving the one-dimensional Schrödinger equation for the barrier model shown in Fig. 2. The real part of the barrier potential is given by

$$\begin{aligned} V_R(z) &= 1/[2(z-z_0)], \quad z \le z_1 \\ &= -U_1 - z/[2(z-z_0)^2], \quad z_1 \le z \le z_c \\ &= -U_0, \quad z \ge z_c \end{aligned} \tag{17}$$

where U_0 is the inner potential of the crystal, U_1 is the barrier height at the top layer of atoms, z_0 is the image barrier origin, z_1 is the point at which saturation begins, and z_c is the point at which the inner potential is reached. The origin is chosen at the nuclear positions of the outermost layer of atoms. Inelastic scattering is represented by an imaginary component of the barrier potential of the form

$$V_{\mathrm{im}}(z) = \begin{cases} V_1\exp(-az^2) & \text{for } z \le 0 \\ V_1 & \text{for } z \ge 0 \ , \end{cases} \tag{18}$$

where the adjustable parameters V_1 and a have the values 0.1 Ry and 0.1 bohr^{-2} in these calculations.[8]

The amplitude reflection and transmission coeffi-

cients for each of the diffracted beams are found by integrating the Schrödinger equation for this one-dimensional barrier from large negative z to a value of z beyond z_c. The appropriate Schrödinger equation is

$$\frac{d^2\psi}{dz^2}+[k_\perp^2-V(z)]\psi=0\,, \tag{19}$$

where $k_\perp$ is the normal component of the $\vec{k}$ vector of the beam in the vacuum and $V(z)$ is the potential given by Eqs. (17) and (18). The solution is started with the asymptotic form of the wave function for the image-potential barrier

$$\psi\rightarrow\xi^\lambda\exp(-\xi/2)\,, \tag{20}$$

where $\xi=2ik_\perp z$ and $\lambda=-i/4k_\perp$. The Numerov algorithm is used to propagate the solution from two starting values in the asymptotic region to a point $z_E>z_c$. The reflection and transmission coefficients for the barrier are then given by

$$\underline{r}^{+-}=\frac{ik_\perp\psi_0+\psi_0'}{ik_\perp\psi_0-\psi_0'}\exp(-2ik_\perp z_E)\,, \tag{21}$$

and

$$\underline{t}^{--}=\frac{2ik_\perp}{ik_\perp\psi_0-\psi_0'}\exp(ik_\perp z_E)\,, \tag{22}$$

where ψ_0 is the value of the wave function at the point z_E. The derivative of the wave function at z_E,ψ_0' is found from the three-point formula

$$\psi_0'=\frac{1}{2h}(3\psi_0-4\psi_{-1}+\psi_{-2})\,. \tag{23}$$

In practice, a starting value of $z\sim-30$ bohr and an integration mesh of $\Delta z=0.05$ bohr give adequate precision in the calculations of $\underline{R}_T^{-+}$. Since previous calculations have provided no evidence for significant external backscattering by the surface barrier, we choose

$$\begin{aligned}&\underline{r}^{-+}=0\,,\\&\underline{t}^{++}=(k_\perp/k_\perp')^{1/2}\,,\end{aligned} \tag{24}$$

where $k_\perp'$ is the normal component of the reflected wave vector in the vacuum region.

IV. COMPARISON BETWEEN THEORY AND EXPERIMENT

A. Fitting procedure

To fit the spin-polarized LEED fine structure we have used the following procedure:

(1) The inner potential U_0 is determined by comparing the observed and calculated Bragg peaks in the specular reflectivity curves. In general, U_0 is a function of energy and on extrapolation to low energies it approaches a value of $(\phi+E_F)$, where ϕ is the work function of the surface and E_F the Fermi energy of the material. We have selected a constant value of $U_0=1$ Ry (13.6 eV) for these calculations, based on an overall fit of the data of Pierce *et al.* near $\theta=20°$. Herlt *et al.* determined a similar value (14.0 eV) by comparing theory and experiment for normal incidence.[23]

(2) The barrier height U_1 and origin z_0 are varied over a reasonable range and the location of the fine structure noted. This yields a table of peak positions as a function of U_1 and z_0.

(3) The best choices of U_1 and z_0 are determined by comparing the experimental data with these results.

(4) The fit is refined by adjusting the inelastic damping and using a fine energy mesh to locate the upper peaks of the Rydberg series.

(5) The above procedure is repeated at several angles of incidence to determine the overall best fit and the surface-barrier structure.

In their calculations on Cu(001), Dietz *et al.*[16] found that a line of barrier parameters in the (z_0,U_1) space gave an equally good fit to the experimental data. In the present calculations, $\underline{R}^{-+}$ is determined exactly from first principles and we found only three small regions in (z_0,U_1) space where a good fit existed. By using the data for several angles of incidence we were able to find an optimum one-dimensional barrier of the saturated-image form.

B. Determination of barrier shape

As discussed in a previous publication,[8] the above procedure was used to test the adequacy of the saturated-image barrier for analyzing the data described in Sec. II. Using the high-resolution data of Adnot and Carette,[19] we could locate three pairs of (z_0,U_1) which provided a good fit. The three barriers are similar in shape and differ by an approximately rigid translation perpendicular to the surface. The spin-polarized LEED data contain a wealth of structure at low energies which then enabled us to test the barrier models thoroughly and determine an overall best fit. One barrier (-3.3 bohr, 0.7 Ry) gave a satisfactory fit to the experimental data, and calculated and measured intensities are shown for $\theta=15°$, 26°, 43°, and 48° in Fig. 4.

It is clear that very good agreement between theory and experiment is obtained, particularly for the Rydberg series near the (01) beam emergence. At lower energies the agreement is also good, although some of the relative peak heights could be

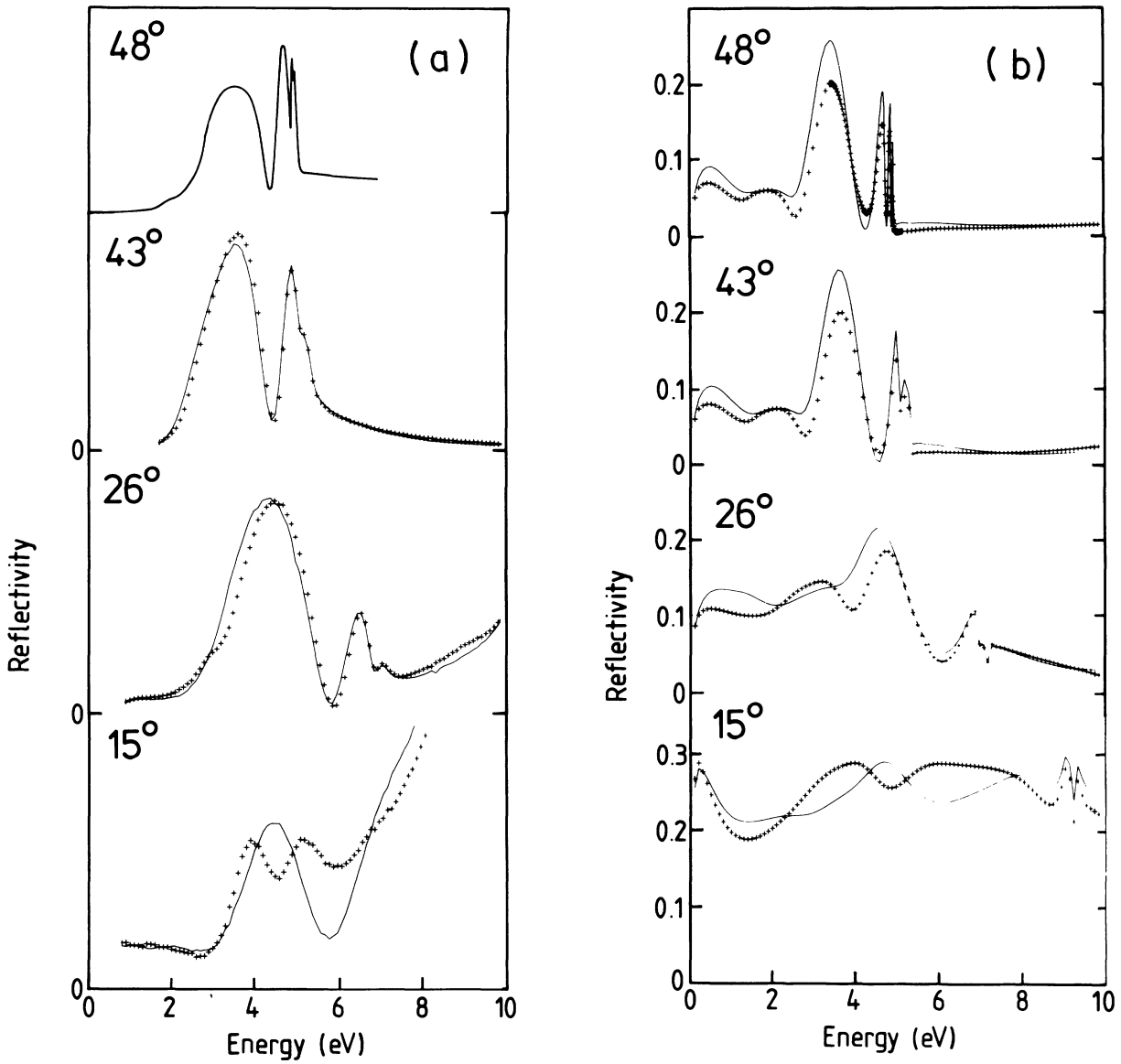

FIG. 4. (a) Experimental data for $\theta=15°$, 26°, 43°, and 48°. The measurements for $\theta=48°$ are from Ref. 19, the remainder from Ref. 6. (b) Corresponding calculations using the saturated-image barrier of Fig. 2. The full curves denote spin-down and the crosses spin-up results, respectively.

improved by adjusting the damping parameters. The sensitivity of the fine-structure peak heights to surface roughness limits their significance, however, and we have not done this. It may be seen that the change in the double-peak structure in the spin-up channel with increasing θ is more pronounced in experiment than in the calculations. The calculations for $\theta=17.5°$, for example, show better agreement with experimental curves with a nominal angle of incidence of 15°. This is consistent with the retarding field method used to vary the energy in Ref. 6.[29]

The saturated-image barrier model thus provides a satisfactory description of the fine structure in these experiments. Other models, such as the modified-image barrier, have been shown to be less satisfactory for the analysis of LEED fine structure on Cu(001).[7] It should be noted that these barriers are special cases of the saturated-image barrier with appropriately chosen parameters. There is no evidence from these calculations for dynamical effects[20] such as an angular or energy dependence of U_1. However, when further high-resolution LEED data with a wider range of θ and energy become available, it may be possible to detect such effects.

V. EXPLANATION OF LOW-ANGLE FINE STRUCTURE

The structure of the low-energy and low-angle specular intensity curves for W(001) has been the subject of considerable analysis and speculation. To determine which features are spin dependent and which barrier dependent, we have performed parallel sets of calculations with and without spin-polarization for both the saturated-image and nonreflecting barriers. In the latter, the internal and external reflection coefficients are neglected and only the transmission coefficients retained.

In Fig. 5, we compare the spin-free and spin-dependent calculations for both barrier models with the normal incidence data of Herlt *et al.*[23] The results show clearly that a broad Bragg peak is present near 6 eV in all calculations and that a secondary Bragg peak near 14 eV is modified by barrier scattering near the (01) beam emergence at 15 eV. Only the spin-dependent calculations give rise to the narrow peak at 3 eV, and this peak is present for both barriers. In agreement with the recent analyses of Willis and Christensen,[30] Herlt *et al.*[23] and McRae *et al.*,[6] the peak may therefore be ascribed to a gap in the spin-dependent band structure. This result demonstrates the need for a spin-dependent model for LEED calculations on substrates with high atomic numbers. It is also interesting that the very low energy peak, clearly resolved in the experiment, is present in both spin-dependent and spin-free calculations for the saturated-image barrier, but absent for the nonreflecting barrier. A shoulder at 11 eV is not reproduced by the present calculations. Herlt *et al.*[23] found that its intensity was significantly enhanced by contraction of the top layer spacing.

The spin-free and spin-dependent calculations with and without barrier scattering are compared with experiment for $\theta=15°$ in Fig. 6. This is an example of a complex fine structure due to emergences interacting with Bragg features. It is again clear that spin-free calculations are quite inadequate and that only the spin-dependent calculation with barrier scattering provides satisfactory agreement with experiment. As noted above, the calculated curve for $\theta=17.5°$ shows improved agreement with the experimental curve for $\theta=15°$ [Fig. 6(a)]. In particular, the second of the peaks in the spin-up curve near 5 eV is much narrower than the corresponding peak in Fig. 6(e).

To complement the data in Fig. 6, we show in Fig. 7 the results of spin-dependent calculations for $\theta=0°$, 5°, 10°, and 26°. The spin-dependent feature at 3–4 eV persists at all these angles, while the Bragg peak moves gradually upwards from 6 eV at normal incidence to about 8 eV at $\theta=15°$. As the

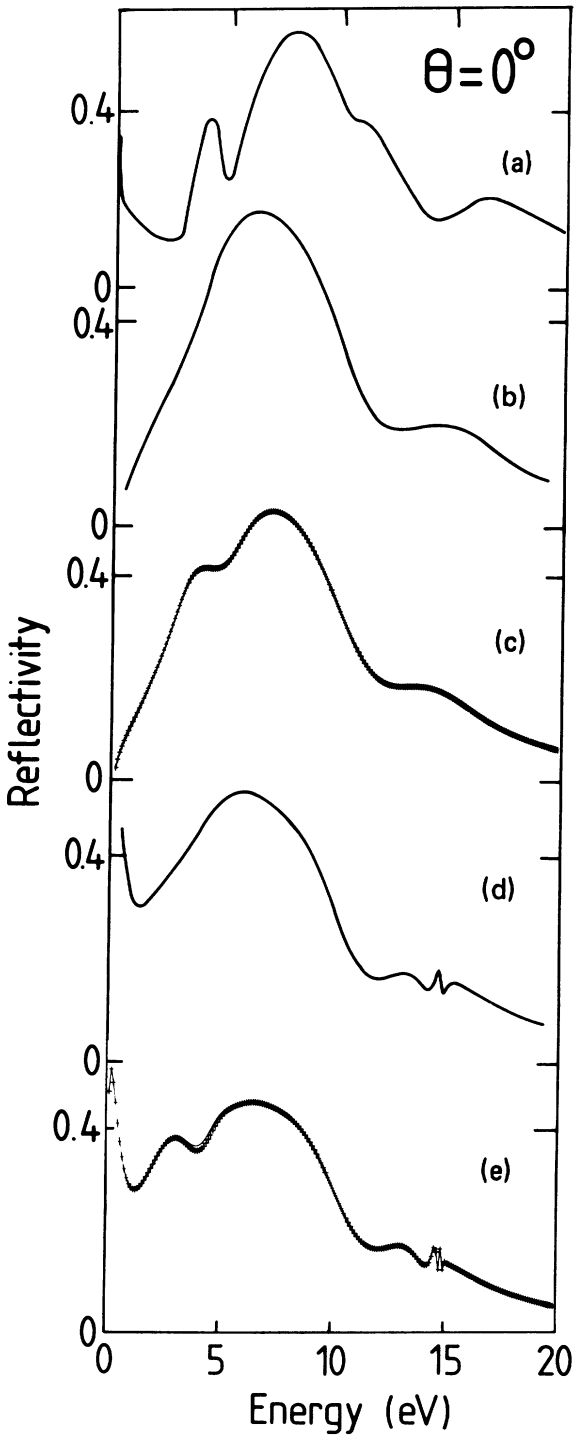

FIG. 5. Results for $\theta=0$. (a) Experimental total reflectivity (Ref. 23). (b) Spin-free, nonreflecting barrier. (c) Spin-dependent, nonreflecting barrier. (d) Spin-free, saturated-image barrier. (e) Spin-dependent, saturated-image barrier. The spin-down (full curve) and spin-up (crosses) results are indistinguishable at normal incidence.

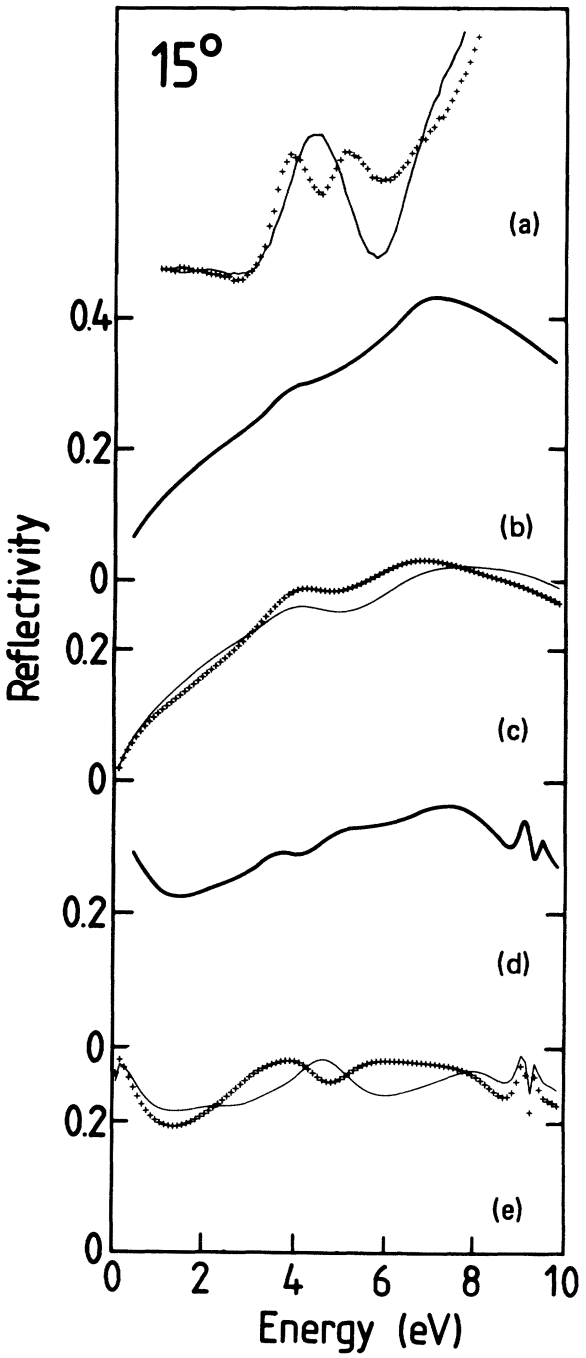

FIG. 6. Results for $\theta=15°$. Curves as in Fig. 5. The experimental curve is from Ref. 6.

emergences of the (10), [(0$\bar{1}$) and (01)], and ($\bar{1}$0) beams separate with increasing θ, the intensity profiles become more complex due to the interaction of the Bragg features and the interference fine structure. At $\theta=10°$, the interaction of the (10) beam emergence with the Bragg peak produces a double-peaked structure which is slightly displaced in the spin-up and spin-down profiles. At $\theta=15°$, an interference peak is superimposed on the Bragg peak and slight shifts in the spin-dependent features near 4 eV produce an interesting double-peaked structure in the spin-up beam. The complexity of the $\theta=15°$ curves can therefore be interpreted as the interaction of interference fine structure with a Bragg peak and the spin-dependent feature at 4 eV. It is not necessary to invoke a new type of feature such as the double resonance of Rundgren and Malmström,[10] which involves the simultaneous emergence of inequivalent beams.

For incident angles above 20° on this azimuth, the (10) threshold lies below the Bragg peak and the fine-structure profiles are dominated by the barrier interferences. As can be seen from Fig. 4, these profiles are much simpler than those for smaller values of θ. The 3-eV spin-dependent peak is still present for $\theta>20°$, but gradually weakens at higher angles of incidence, as shown in Fig. 4(b).

VI. CONCLUDING REMARKS

The saturated-image barrier of Fig. 2 ($z_0=-3.3$ bohr, $U_1=0.7$ Ry) gives a satisfactory description of the spin-polarized LEED fine structure for energies below 10 eV over the entire range of incident angles from normal incidence to $\theta=48°$. The present data provide no evidence for dynamical effects, such as an angle or energy dependence of U_1, but this would be an interesting aspect in the analysis of future data of higher-resolution and different energy ranges.

It is interesting to note that the barriers which reproduce the fine structure in[16] Cu(001) are approximately rigid translations of each other. This is also true of the three barriers which reproduce the fine-structure splittings in W(001) at $\theta=48°$, i.e., the distance between z_0 and the point where the barrier joins the bulk inner potential is approximately 7 bohr in each case. This is a similar length scale to that found in jellium calculations for $r_s=2$,[31] where the barrier changes predominantly over the range of the Fermi wavelength ($2\pi/k_F$). For this value of r_s, Lang and Kohn[21] also found that z_0 lies 1.6 bohr outside the positive background [3.1 bohr from the outermost layer for W(001)] and that the position where the barrier is halfway between its bulk and vacuum values is near the edge of the positive background. Although a comparison between a transition-metal surface and a jellium model must be treated with caution, qualitative similarities between the jellium results and the barrier of Fig. 2 are evident.

The saturated-image barrier is able to explain all

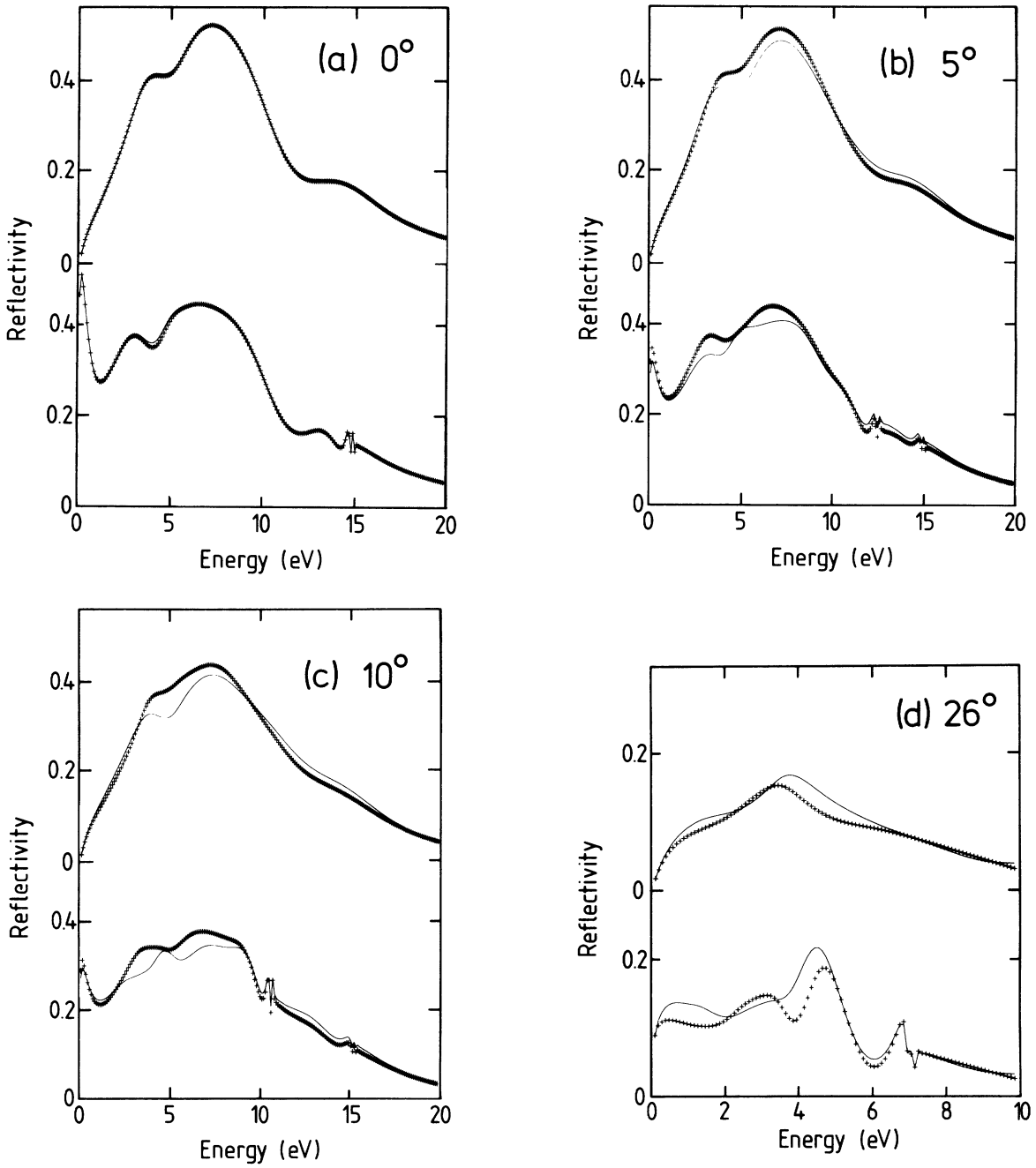

FIG. 7. Spin-dependent LEED intensity calculations for W(001). (a) $\theta=0°$ (b) $\theta=5°$ (c) $\theta=10°$ (d) $\theta=26°$. In each case the upper curve is for the nonreflecting barrier and the lower curve for the saturated-image barrier. Spin-down and spin-up results are given by full curves and crosses, respectively.

the observed fine structure in the rather complex set of spin-polarized LEED intensity curves for W(001). For $\theta<20°$, the interaction of Bragg peaks and emergence features provides a demanding test for the theory. At higher incident angles, only the emergence features are present and the agreement between theory and experiment is very good. Even with pseudorelativistic phase shifts, however, the spin-free model does not provide a satisfactory picture of the LEED fine structure at low angles of incidence. This shows that spin-dependent calculations are essential in LEED studies of systems with

high atomic numbers.

The low-energy electron reflectance from W(001) has been the subject of considerable dispute for more than a decade. The present work shows that satisfactory agreement between theory and experiment can be obtained by the inclusion of relativistic effects and a saturated-image model of the potential barrier.

ACKNOWLEDGMENTS

J. D. Carette and D. T. Pierce provided the original data of Refs. 19 and 6, respectively. It is a pleasure to thank them and also R. Baudoing and E. G. McRae for helpful discussions and correspondence.

[1]D. T. Pierce, R. J. Celotta, G.-C. Wang, W. N. Unertl, A. Galejs, C. E. Kuyatt, and S. R. Mielczarek, Rev. Sci. Instrum. 51, 478 (1980).

[2]J. Kirschner and R. Feder, Phys. Rev. Lett. 42, 862 (1979).

[3]P. J. Jennings, Surf. Sci. 20, 18 (1970).

[4]R. Feder, Phys. Status. Solidi B 46, K31 (1971).

[5]See, for example, R. Feder, J. Phys. C 14, 2049 (1981), and references therein.

[6]D. T. Pierce, R. J. Celotta, G.-C. Wang, and E. G. McRae, Solid State Commun. 39, 1053 (1981); E. G. McRae, D. T. Pierce, G.-C. Wang, and R. J. Celotta, Phys. Rev. B 24, 4230 (1981). For measurements at higher energies, see G.-C. Wang, B. I. Dunlap, R. J. Celotta, and D. T. Pierce, Phys. Rev. Lett. 42, 1349 (1979).

[7]P. J. Jennings, S. M. Thurgate, and G. L. Price, Appl. Surf. Sci. 13, 180 (1982).

[8]P. J. Jennings and R. O. Jones, Solid State Commun. 44, 17 (1982).

[9]E. G. McRae and G. H. Wheatley, Surf. Sci. 29, 342 (1972).

[10]G. Malmström and J. Rundgren, J. Phys. C 14, 4937 (1981).

[11]E. G. McRae, Rev. Mod. Phys. 51, 541 (1979).

[12]E. G. McRae, Surf. Sci. 25, 491 (1971).

[13]J. Rundgren and G. Malmström, Phys. Rev. Lett. 38, 836 (1977); J. Phys. C 13, L61 (1981).

[14]P. M. Echenique and J. B. Pendry, J. Phys. C 11, 2065 (1978).

[15]J. C. Le Bosse, J. Lopez, C. Gaubert, Y. Gauthier, and R. Baudoing, J. Phys. C 15, 3425 (1982); 15, 6087 (1982). The latter paper provides more details and emphasizes the inadequacy of a description of threshold effects in terms of resonances.

[16]R. E. Dietz, E. G. McRae, and R. L. Campbell, Phys. Rev. Lett. 45, 1280 (1980).

[17]P. J. Jennings and R. O. Jones, Surf. Sci. 71, 101 (1978).

[18]P. J. Jennings, Surf. Sci. 75, L773 (1978); 88, L25 (1979); S. M. Thurgate and P. J. Jennings, *ibid.* 114, 395 (1982).

[19]A. Adnot and J. D. Carette, Phys. Rev. Lett. 38, 1084 (1977).

[20]See, for example, J. Harris and R. O. Jones, J. Phys. C 6, 3585 (1973); 7, 3751 (1974); C. H. Hodges, *ibid.* 8, 1849 (1975).

[21]N. D. Lang and W. Kohn, Phys. Rev. B 7, 3541 (1973).

[22]I. H. Khan, J. P. Hobson, and R. A. Armstrong, Phys. Rev. 129, 1513 (1963); R. A. Armstrong, Surf. Sci. 47, 666 (1975).

[23]H.-J. Herlt, R. Feder, G. Meister, and E. G. Bauer, Solid State Commun. 38, 973 (1981).

[24]K. Kambe, Z. Naturforsch. 22a, 322 (1967); 23a, 1280 (1968).

[25]E. G. McRae, Surf. Sci. 11, 479 (1968).

[26]L. F. Mattheiss, Phys. Rev. 139, 236 (1965).

[27]P. J. Bunyan and J. L. Schonfelder, Proc. Phys. Soc. 85, 455 (1965).

[28]R. Feder, P. J. Jennings, and R. O. Jones, Surf. Sci. 61, 307 (1976).

[29]E. G. McRae and D. T. Pierce (private communication) showed that this method underestimates the true angle of incidence by 1–2° for 4-eV electrons with a nominal angle of incidence of 15°, and by 2–3° for a nominal θ of 20°.

[30]R. F. Willis and N. E. Christensen, Phys. Rev. B 18, 540 (1978); R. F. Willis, in *Vibrations of Surfaces,* edited by R. Caudano, J. M. Gilles, and A. A. Lucas (Plenum, New York, 1982).

[31]N. D. Lang and W. Kohn, Phys. Rev. B 1, 4555 (1970).